Carbohydrate Polymers 120 (2015) 60–68

Contents lists available at ScienceDirect

Carbohydrate Polymers

journal homepage: www.elsevier.com/locate/carbpol

Novel one-pot synthesis of dicarboxylic acids mediated alginate–zirconium biopolymeric complex for defluoridation of water

Subbaiah Muthu Prabhu, Sankaran Meenakshi*

Department of Chemistry, The Gandhigram Rural Institute, Deemed University Gandhigram, 624302, Dindigul, Tamil Nadu, India

ARTICLE INFO

Article history:
Received 7 October 2014
Received in revised form
19 November 2014
Accepted 27 November 2014
Available online 3 December 2014

Keywords:
Sodium alginate
Zirconium
Dicarboxylic acid
Fluoride
Adsorption

ABSTRACT

The present investigation explains the fluoride removal from aqueous solution using alginate–zirconium complex prepared with respective dicarboxylic acids like oxalic acid (Ox), malonic acid (MA) and succinic acid (SA) as a medium. The complexes viz., alginate–oxalic acid–zirconium (Alg–Ox–Zr), alginate–malonic acid–zirconium (Alg-MA-Zr) and alginate–succinic acid–zirconium (Alg–SA–Zr) were synthesized and studied for fluoride removal. The synthesized complexes were characterized by FTIR, XRD, SEM with EDAX and mapping images. The effects of various operating parameters were optimized. The result showed that the maximum removal of fluoride 9653 mgF^-/kg was achieved by Alg–Ox–Zr complex at acidic pH in an ambient atmospheric condition. Equilibrium data of Alg–Ox–Zr complex was fitted well with Freundlich isotherm. The calculated values of thermodynamic parameters indicated that the fluoride adsorption is spontaneous and endothermic in nature. The mechanism of fluoride removal behind Alg–Ox–Zr complex has been proposed in detail. The suitability of the Alg–Ox–Zr complex has been tested with the field sample collected in a nearby fluoride endemic area.

© 2014 Elsevier Ltd. All rights reserved.

1. Introduction

Fluoride is recognized worldwide as one of the most serious inorganic pollutants in drinking water. Though the low concentration range (<1.5 mg/L) in drinking water, fluoride strengthens the tooth enamel and also take part in a large variety of cellular processes (Barbier, Arreola-Mendoza, & Razo, 2010; Cao et al., 2013; Mohapatra, Anand, Mishra, Giles, & Singh, 2009; Vani & Reddy, 2000; Viswanathan & Meenakshi, 2008). Concentrations in the range of (>1.5 mg/L) result in dental fluorosis, whereas with prolonged exposure at still higher fluoride concentrations, dental fluorosis progresses to skeletal fluorosis. Therefore the World Health Organization as well as many countries has set the maximum fluoride concentration in drinking water as 1.5 mg/L (WHO, 2006). Though several methods have been adopted for fluoride removal from aqueous solution, adsorption is a helpful method for fluoride removal, as it can be implemented using gravity and in terms of low cost, high efficiency, ease of reuse and operation.

Alginate is a biopolymer and polysaccharide composed of different proportions of β-D-mannuronic acid and α-L-guluronic acid units, linked by β-1-4 and α-1-4 bonds. Among the various natural polymers, sodium alginate (Alg) is widely used biopolymer next to chitosan for various metal ions removal (Park & Chae, 2004), membrane preparation (Kurkuri, Kumbar, & Aminabhavi, 2002), sensing applications (Polyak, Geresh, & Marks, 2004) and dye removal (Trandafilović et al., 2014) due to its unique properties. Only a few materials have been proposed for fluoride removal mechanism with alginate biopolymers as pillared like support viz., aluminum alginate particles (Lee & Mooney, 2012), alginate based anion exchanger (Paudyal et al., 2013) nano-hydroxyapatite encapsulated alginate (Pandi & Viswanathan, 2014), lanthanum alginate beads (Yakun, Wenming, Xia, Jingnian, & Menghua, 2011), alginate entrapped mixed metal oxides (Swaina, Patnaik, Patnaik, Jha, & Dey, 2013) alumina entrapped alginate beads (Basu, Singhal, Pimple, & Reddy, 2013) and glutaraldehyde cross-linked alginate (Vijaya, Popuri, Reddy, & Krishnaiah, 2011). Moreover, several metals have been adopted for complexation reaction with fluoride and zirconium is the highlighted metal as it has chemical stability with fluoride due to strong affinity, binding tendency and less leaching effect (Ramosa, Utrilla, Castilloa, & Polo, 2010). Also, dicarboxylic acid like oxalic acid has demonstrated a positive effect on the reduction of particle size during complexation and aggregation step (Pettibone, Cwiertny, Sherer, & Grassian, 2008; Ketabi, Kazemi, & Mohagheghi, 2011). Especially in this study, oxalic acid is complexed with zirconium ions which control the growth of ZrO_2

* Corresponding author. Tel.: +91 451 2452371; fax: +91 451 2454466.
E-mail address: drs_meena@yahoo.co.in (S. Meenakshi).

http://dx.doi.org/10.1016/j.carbpol.2014.11.058
0144-8617/© 2014 Elsevier Ltd. All rights reserved.

particles that reduce the dispersion in this method. In addition to oxalic acid, malonic acid and succinic acid are also practiced for the complexation with alginate and zirconium.

In this present endeavor, novel complexes, Alg–Ox–Zr, Alg–SA–Zr and Alg–MA–Zr, have been synthesized by a single-pot method using Ox, SA and MA respectively, as a medium with the biomaterial alginate for fluoride removal studies. The synthesized complex has been characterized by FTIR, XRD, SEM with EDAX and mapping studies. The defluoridation studies includes the effect of stirring time, the effect of pH, competitor anions, as well as the effect of temperature has been carried out by batch equilibrium model. A comparative study has been made for Zr–Ox and Alg–Ox–Zr complex for evaluating fluoride removal capacity using the adsorption method by keeping all the parameters as constant. In order to check the viability of fluoride removal using other dicarboxylic acids like MA and SA have been tested and compared with a few adsorbents of fluoride uptake studies. The mechanism of fluoride removal by Alg–Ox–Zr complex has been illustrated in detail.

2. Materials and methods

2.1. Materials

Sodium alginate, acrylamide (99%), oxalic acid, malonic acid, succinic acid and zirconium oxychloride were purchased from Central Drug House (CDH), New Delhi and all other chemicals and reagents used were of analytical grade. All the solutions were prepared using double distilled water.

2.2. Synthesis of Zr–Ox and Alg–Ox–Zr complex

The Alg–Ox–Zr complex adsorbent for fluoride removal was successfully synthesized by single-pot process through the co-precipitation method (Muthu Prabhu & Meenakshi, 2015; Sundaram & Meenakshi, 2009). About 2 g of sodium alginate was dissolved in 100 mL of distilled water at 40 °C in a three necked round bottom flask and stirred continuously for 6 h by keeping constant temperature and then added 0.1 M zirconium oxychloride solution drop wise with constantly stirring for 40 min. The concentration of oxalic acid was optimized by trial and error method and 0.2 M was found to be effective and hence, added 0.2 M oxalic acid by drop wise for about 120 min. A dirty white color gel-like precipitate was formed. The hot flask was cooled to room temperature for 4 h for the precipitate to settle down. The precipitate was filtered and washed with plenty of water to remove any impurities, and dried at 50 °C in an oven. The dried Alg–Ox–Zr complex adsorbent was used for the experiments. The same concentration and conditions of zirconium and oxalic acid was used for the synthesis of Zr–Ox complex for comparing its capacity with Alg–Ox–Zr complex. The same procedure followed for the synthesis of Alg–Ox–Zr complex was used in the preparation of the complexes like Alg–MA–Zr and Alg–SA–Zr using MA and SA as medium respectively.

2.3. Sorption experiments

In a typical case, a known amount of the sorbent was added to 100 mL of NaF solution with an initial concentration of 10 mg/L. The contents were shaken thoroughly using a thermostated shaker rotating at a speed of 200 rpm and the filtrate was analyzed for fluoride. The influence of various parameters like contact time, pH and the presence of other anions on DC of the sorbents were investigated by varying one parameter at a time and keeping the remaining other parameters as constant. For the temperature studies, the effect of initial fluoride concentrations viz., 8, 10, 12 and 14 mg/L at 303, 313 and 323 K on sorption rate was studied by keeping the mass of the sorbent and volume of solution as 100 mL at neutral pH. The solution was then filtered and the residual fluoride ion concentration was measured.

2.4. Analysis

Expandable ion analyzer EA 940 (Orion, USA) with ion selective fluoride electrode BN 9609 (Orion, USA) was used for the quantitative analysis of fluoride (Fluoride, 2005). The pH measurements were done with the same instrument with pH electrode. All other water quality parameters were analyzed by using standard methods (APHA, 2005). FTIR spectra were recorded on a JASCO-460 FT-IR spectrometer as KBr background. The scanning electron microscope (SEM) images were taken using the Vega3 Tescan model and elemental spectra were obtained using an energy dispersive X-ray analyzer (EDAX) and mapping images were taken during SEM observations which allow qualitative detection and localization of elements present in the complex by Bruker Nano GMBH, Germany. X-ray diffraction (XRD) measurements were obtained using X'per PRO model-PANalytical to determine the crystalline phases present in sorbents.

2.5. Sorption isotherms

Three commonly used isotherms namely Freundlich (Freundlich, 1906), Langmuir (Langmuir, 1916) and D–R isotherm (Milmile et al., 2011) have been adopted to quantify the DC of the complexes and the linear forms of three isotherms were tabulated in Table S1.

In Table S1, q_e is the amount of fluoride adsorbed per unit weight of the sorbent (mg/g), C_e is the equilibrium concentration of fluoride in solution (mg/L), k_F is a measure of adsorption capacity and $1/n$ is the adsorption intensity. The linear plot of $\log q_e$ vs. $\log C_e$ indicates the applicability of Freundlich isotherm. The values of $1/n$ are lying between 0 and 1 and the n value lying in the range of 1–10 confirms the conditions favorable for adsorption. In the Langmuir isotherm, Q^o is the amount of adsorbate at complete monolayer coverage (mg/g) and gives the maximum sorption capacity of sorbent and b (L/mg) is Langmuir isotherm constant that relates to the energy of adsorption. The Langmuir constants Q^o and b were calculated from the respective slope and intercept of plot C_e/q_e vs. C_e respectively. The essential characteristics of the Langmuir isotherm can be expressed in terms of a dimensionless constant separation factor or equilibrium parameter, R_L (Weber & Chakravorti, 1974). In D–R isotherm, X_m is the adsorption capacity (mg/g) and k is the constant related to adsorption energy (mol^2/kJ^2). The respective values of k and X_m were computed from the slope and intercept of the plot $\ln q_e$ vs. ε^2. The magnitude of E value lying between 1–8 and 8–16 kJ/mol indicates the type of adsorption follows physisorption/ion exchange respectively.

2.6. Non-linear analysis

To identify the best isotherm model among the models adopted for the quantification of sorption of fluoride on Alg–Ox–Zr and Zr–Ox complex, regression correlation coefficient (r), chi-square (χ^2) analysis and standard deviation (sd), the sum of the absolute errors (SAE), the average relative error (ARE) and the hybrid fractional error (HYBRID) function of non-linear analysis (Ho, Chiu, & Wang, 2005; Kundu & Gupta, 2006) have been carried out. The equivalent mathematical statements are tabulated in Table S1.

2.7. Thermodynamic treatment

Thermodynamic parameters associated with the adsorption viz., standard free energy change (ΔG^o), standard enthalpy change (ΔH^o), standard entropy change (ΔS^o) were calculated using Khan

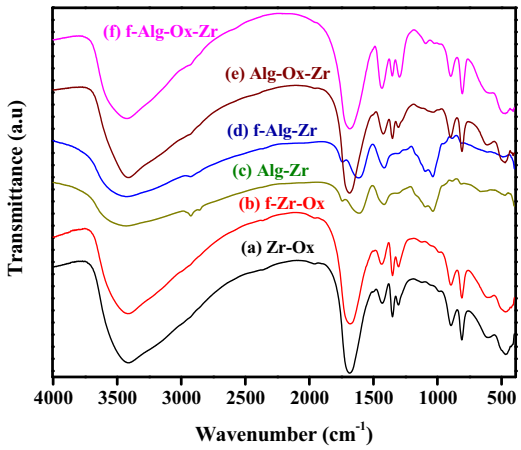

Fig. 1. FTIR spectra of (a) Zr–Ox (b) f–Zr–Ox (c) Alg–Zr (d) f–Alg–Zr (e) Alg–Ox–Zr and (f) f-Alg–Ox–Zr complex.

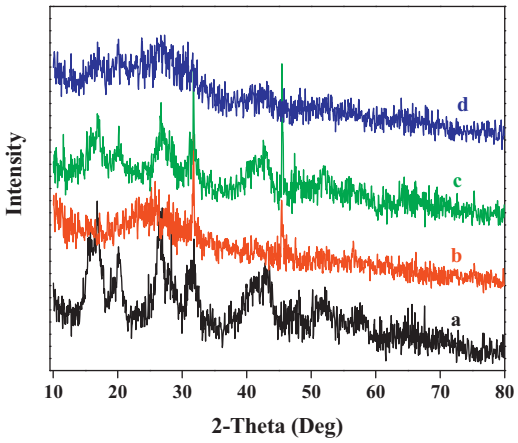

Fig. 2. XRD spectra of (a) Zr–Ox (b) Zr–Alg (c) Alg–Ox–Zr and (d) f–Alg–Ox–Zr complex.

and Singh method (Horsfall & Spiff, 2005; Khan & Singh, 1987). The sorption distribution coefficient may be expressed in terms of standard enthalpy change (ΔH^o) and standard entropy change (ΔS^o) as a function of temperature. The values of ΔH^o and ΔS^o can be obtained from the slope and intercept of the plot of $\ln K_o$ vs. $1/T$.

3. Results and discussion

3.1. Characterization of the adsorbents

3.1.1. FTIR analysis

Fig. 1a and b shows the FTIR images of Zr–Ox and fluoride sorbed Zr–Ox (f–Zr–Ox) complexes, respectively. FT-IR spectra of Zr–Ox show a broad peak at 3407 cm^{-1} which indicate the presence of —OH functional groups. A strong, broad band was observed at 1685 cm^{-1} for —OH bending vibration. The peak at 1350 cm^{-1} indicates the bending vibration of Zr—OH groups. The normal modes peaks at 984, 1120 and 1350 cm^{-1}, are due to the presence of oxalic acid (Jimenez, Hurt, Matos, & Mendez, 2014). The band at 609 cm^{-1} should be assigned to Zr—O bond in the formation of complexes with oxalic acid (Guo & Chen, 2004). After fluoride treatment (Fig. 1b), the band at 3407 cm^{-1} was shifted to 3443 cm^{-1} which may be due to the presence of fluoride in the complex.

Fig. 1c and d shows the FTIR spectra of Zr–Alg and f–Zr–Alg complex, respectively. The FTIR spectra of Alg–Ox–Zr and f–Alg–Ox–Zr respectively are shown in Fig. 1e and f. The FTIR spectrum of Alg–Ox–Zr shows a broad band in the region 3410 cm^{-1} which is probably due to the presence of —OH stretching vibration and the peaks at 1633 cm^{-1} indicated the presence of —OH bending vibration of the complex. A very small peak around 2920 cm^{-1} is due to the stretching vibration of $-CH_2$ groups. The sharp peak at 1350 cm^{-1} is attributed to the bending vibration of Zr—OH bands. A weak vibration band in the range of wavenumber at 1031 cm^{-1} depicts the presence of Zr=O from zirconyl group of the complex. A band at 894 cm^{-1} was assigned to Zr—O. A peak observed at 472 cm^{-1} in case of Alg–Ox–Zr complex is assigned to the monoclinic and tetragonal phase of ZrO_2 (Socrates, 2001). A strong Zr–O–C vibration peak was observed at 810 cm^{-1} is due to the formation of zirconium with alginate complex. The peak at 1424 cm^{-1} was an artifact caused by CO_2 during the complex formation (Cheng, Yasukawa, Kandori, & Ishikawa, 1998). After fluoride treatment (Fig. 1f), the peak at 472 cm^{-1} for ZrO_2 has been shifted to 484 cm^{-1} and slight widening of the band at 3410 cm^{-1} to 3423 cm^{-1} confirms the presence of fluoride in the complex.

3.1.2. XRD studies

The adsorption of fluoride by Zr–Ox and Alg–Ox–Zr complex has been confirmed by XRD study. Fig. 2 illustrates the XRD plots of (a) Zr–Ox, (b) Zr–Alg, (c) Alg–Ox–Zr and (d) f–Alg–Ox–Zr complex. From Fig. 2a, the presence of two peaks in the position of 26.54° (d = 3.35616) and 43.0° (d = 2.09785) which corresponds to monoclinic and the characteristic peak at 32.0° (d = 2.82087) indicates the presence of tetragonal phases of zirconia structures (Koji & Ohgai, 2001). Fig. 2b depicts the XRD spectra of Zr–Alg complex and showed the characteristic peaks of 31.73° (d = 2.81778) and 45.42° (d = 1.99532). Whereas for Alg–Ox–Zr complex (Fig. 2c), the main peaks of 16.96° (d = 5.22340), 20° (d = 4.40649), 27° (d = 3.32550), 31.74° (d = 2.81648), 43° (d = 2.10699), 45.493° (d = 1.99223) and 51.9° (d = 1.76073) which clearly indicates the presence of oxalic acid along with the alginate polymer. After fluoride treatment, (Fig. 2d), the f–Alg–Ox–Zr complex showed the characteristic peak at the position of 18° (d = 4.98420) and 20.03° (d = 4.42946), which clearly indicates the slight changes in the crystalline nature. This may be due to the coordination of fluoride in the Alg–Ox–Zr complex.

3.1.3. SEM with EDAX

The SEM micrographs of Zr–Ox and f–Zr–Ox complex shows morphological changes occur as shown in Fig. 3a and b respectively. Fig. 3a shows the surface of the particles is smooth, clear and not aggregated particles. But after treatment with fluoride, the particles are not smooth and the surface is covered fully. Also, the individual particles are collapsed and this is due to the presence of fluoride domination. The presence of fluoride peak in the EDAX spectrum supports the above statement. Moreover, the percentage of oxygen content is reduced in the EDAX spectrum of fluoride treated Zr–Ox complex than untreated Zr–Ox complex which supports the replacement of hydroxide ion by fluoride ions (Fig. 3d).

Fig. 4a depicts the SEM images of zirconium–oxalic acid complex onto the alginate surface. The alginate polymer plays a pillar like support for the zirconium–oxalic acid complex. After fluoride treatment (Fig. 4b), the surface of the complex is not smooth and clear. Fig. 4c and d indicates the EDAX spectrum of Alg–Ox–Zr complex before and after treatment of fluoride respectively. In the EDAX spectrum of f–Alg–Ox–Zr complex, the presence of fluoride peak and the reduction in oxygen percentage of the EDAX spectrum of f–Alg–Ox–Zr than observed in the raw Alg–Ox–Zr complex confirms the ion-exchange mechanism (Fig. 4d).

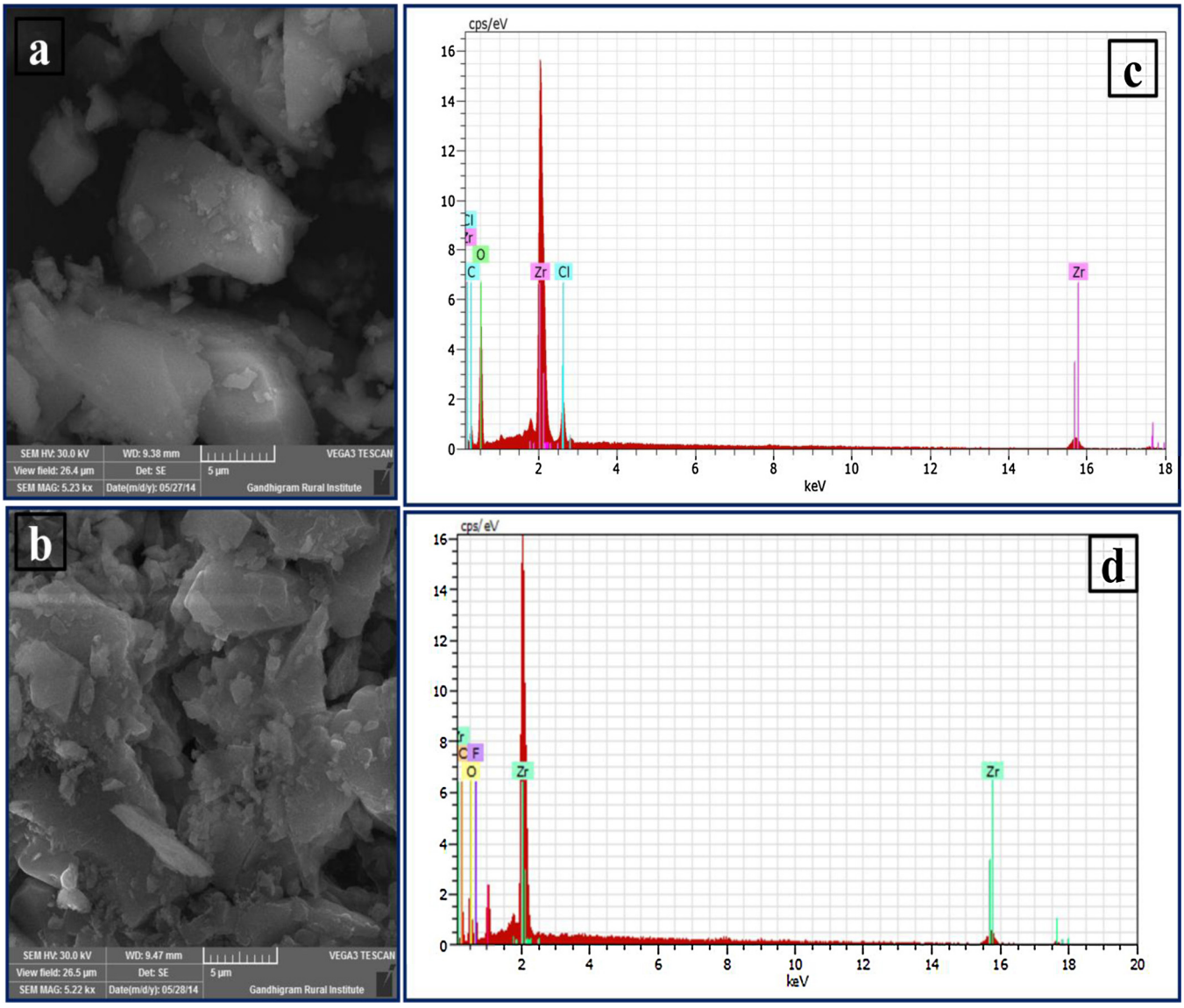

Fig. 3. SEM micrographs of (a) Zr–Ox and (b) f–Zr–Ox complex.

3.1.4. *Mapping images*

Mapping images are used to explain the fluoride adsorption onto Alg–Ox–Zr complex before and after treatment and are shown in Fig. 5a and b respectively. Fig. 5a represents the presence of corresponding elements of Alg–Ox–Zr complex by its own color. After treatment with fluoride (Fig. 5b), the dominance of blue color which represents the presence of fluoride along with other elements indicates the fluoride sorption onto Alg–Ox–Zr complex.

3.2. *Influence of contact time*

The influence of contact time on the DC of Zr–Ox, Alg–Zr, Alg–Ox–Zr, Alg–MA–Zr and Alg–SA–Zr complexes by keeping the fluoride concentrations as 10 mg/L and dose as 50 mg at ambient temperature are shown in Fig. S1. As shown in Fig. S1, the DC increases initially from 5 min, reached saturation at 25 min and then it remains constant upto 40 min. Hence, further studies were carried out by fixing the contact time as 25 min in order to avoid sorption error. The maximum DC of Alg–Ox–Zr, Zr–Ox, Alg–Zr, Alg–MA–Zr and Alg–SA–Zr complexes were found to be 9653, 5376, 5297, 4851 and 4059 mgF^-/kg, respectively. Among all the adsorbents, Alg–Ox–Zr complex experienced higher DC than the other complexes. The Alg–MA–Zr and Alg–SA–Zr complexes showed lower DC than oxalic acid complexes which may be due to the presence of more alkyl groups which leads to steric hindrance. Hence, further studies were limited only with Alg–Ox–Zr complex and have been compared with Zr–Ox complex.

3.3. *pH studies*

The effect of pH on fluoride removal by Alg–Ox–Zr and Zr–Ox complexes was investigated in the pH range of 3–11 by keeping all other parameters as constant and the results are displayed in Fig. S2. The fluoride removal was highly pH dependent and peaked at pH 3–6, above which the fluoride removal decreased with the increasing pH. The maximum DC of 9651 mgF^-/kg was occurred at pH 3 for Alg–Ox–Zr complex and 5840 mgF^-/kg for the Zr–Ox complex. At basic condition, the DC is significantly reduced, which may be due to the presence of more hydroxide ions which would disturb fluoride ionic exchange.

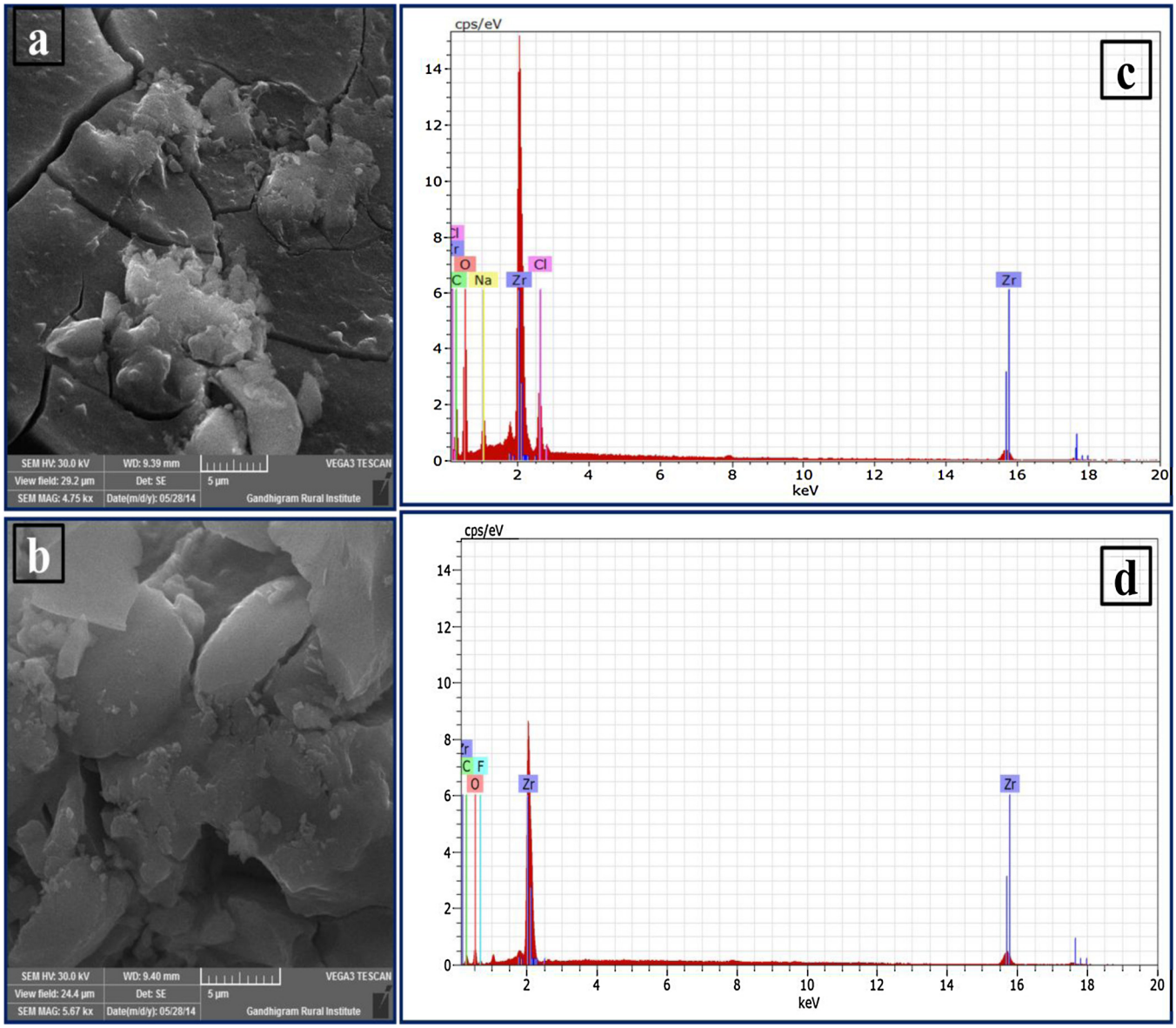

Fig. 4. SEM micrographs of (a) Alg–Ox–Zr and (b) f–Alg–Ox–Zr complex.

3.4. Competitor ions

In the natural systems, several anions can complete for adsorption sites of Alg–Ox–Zr and Zr–Ox complexes. Therefore, the effects of various competitive anions on the uptake of fluoride from aqueous solutions were investigated. The effects of the co-existing anions, including chloride, nitrate, sulphate and bicarbonate, with the fixed concentrations of 200 mg/L were investigated as shown in Fig. S3, which demonstrated that the presence of bicarbonate significantly decreased the DC when compared to other co-ions. This may be due to the release of $-OH^-$ ions from the hydrolysis of $NaHCO_3$ which increase the solution pH which in turn decrease the DC.

3.5. The best fit sorption isotherms using linear and error analysis method

The Freundlich isotherm constants $1/n$ and k_F; the Langmuir constants Q^o and b; the values of D–R isotherm constants k and X_m were calculated and tabulated in Table 1. The increasing values of Q°, and decreasing b and k_F with respect to temperature confirms the ion-exchange between the sorbents and fluoride (Meenakshi & Viswanathan, 2007). The value of E from D–R isotherm lying between 8 and 16 kJ/mol, once again confirms the existence of the ion-exchange between sorbent and fluoride. The best fit isotherm was identified using the non-linear and error analysis data. The results of chi-square, SAE, ARE and HYBRID analysis for all the isotherms were tabulated in Table 1. Based on the above said values, the best isotherm fit was arrived in the order as: Freundlich > > D–R > Langmuir for fluoride sorption by Alg–Ox–Zr and Freundlich > > Langmuir > D–R for Zr–Ox complex and hence fluoride sorption by both the sorbents follows Freundlich isotherm which indicates the heterogeneous nature of the sorption.

3.6. Thermodynamic treatment of the sorption process

The values of thermodynamic parameters are shown in Table 2. The negative values of ΔG° for both Alg–Ox–Zr and Zr–Ox

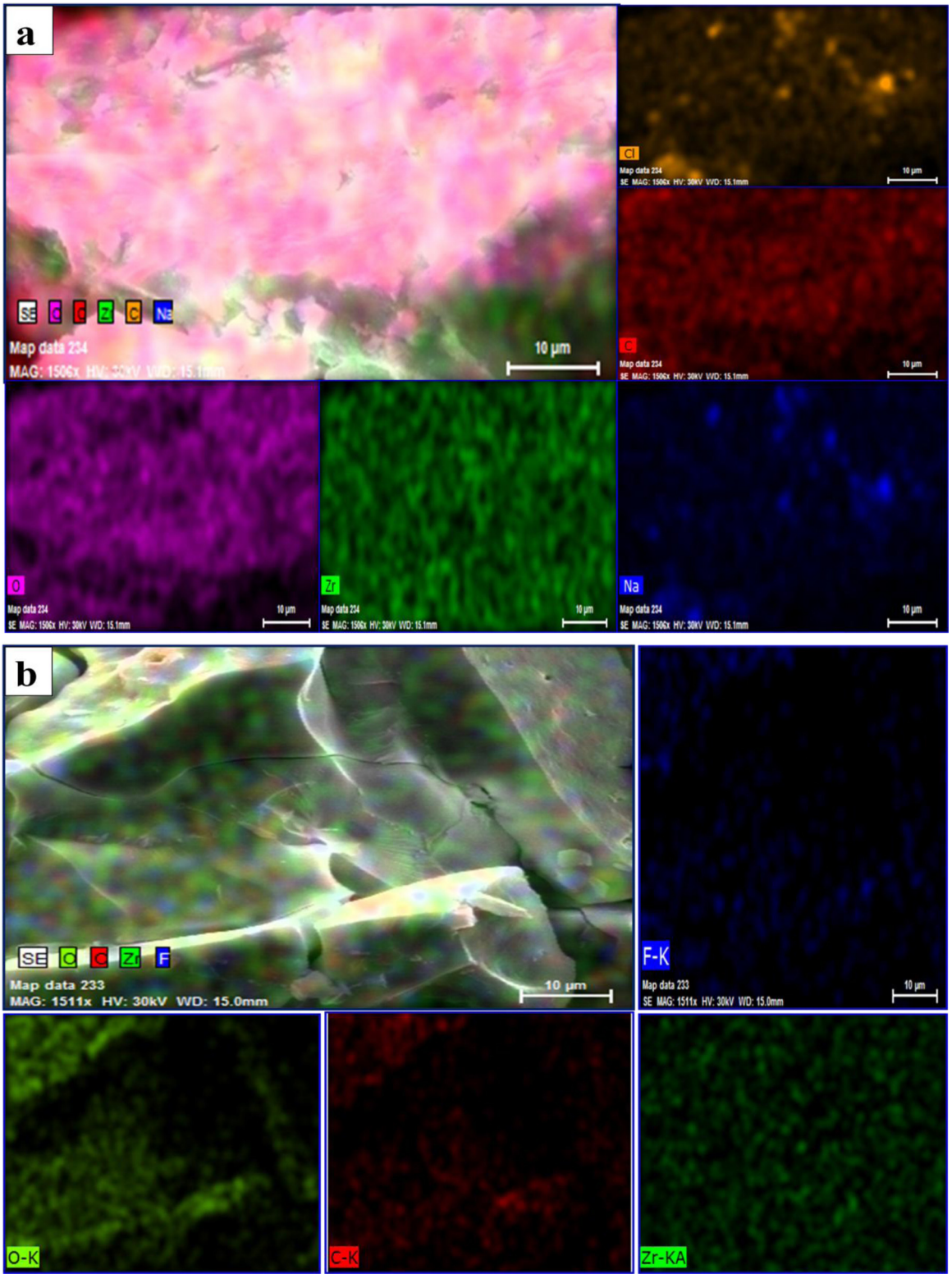

Fig. 5. Mapping images of (a) Alg–Ox–Zr and (b) f–Alg–Ox–Zr complex.

complexes confirm the spontaneous nature of fluoride removal. The value of ΔH° is positive, indicating that the sorption process is endothermic for both the complexes. Moreover, the positive value of ΔS° which is a measure of randomness at the solid/liquid interface during fluoride sorption indicates that the fluoride sorption is irreversible and stable.

3.7. Sorption kinetics

The two types of kinetic models viz., reaction-based and diffusion-based models were applied to test the fitness of experimental data for both Alg–Ox–Zr and Zr–Ox complexes (Ho, Ng, & McKay, 2000).

Table 1
Isotherms calculations of Zr–Ox and Alg–Ox–Zr complex.

Isotherms	Parameters	Zr–Ox			Alg–Ox–Zr		
		303 K	313 K	323 K	303 K	313 K	323 K
Freundlich	$1/n$	0.135	0.160	0.173	0.122	0.135	0.141
	n	7.330	6.228	5.730	7.436	7.769	8.012
	$k_{F\ (mg/g)\ (L/mg)^{1/n}}$	5.050	4.795	4.455	6.305	6.413	6.981
	r^2	0.960	0.965	0.978	0.997	0.996	0.995
	sd	0.016	0.013	0.015	0.018	0.015	0.016
	χ^2	3.3E – 3	3.6E – 3	2.2E – 3	5.2E – 3	4.3E – 3	6.0E – 3
	SAE	7.9E – 3	7.8E – 3	6.7E – 3	8.1E – 3	9.5 E – 3	1.2E – 3
	ARE	1.4E – 2	1.2E – 2	9.2E – 3	0.010	0.012	0.015
	HYBRID	0.095	0.091	0.058	0.130	0.109	0.152
Langmuir	Q^o(mg/g)	5.970	6.025	6.179	9.372	9.462	9.579
	b (L/g)	7.075	4.872	3.677	7.345	6.598	5.719
	R_L	0.012	0.013	0.017	5.4E – 3	6.7E – 3	1.4E – 2
	r^2	0.837	0.868	0.883	0.956	0.924	0.893
	sd	0.016	0.018	0.019	0.064	0.079	0.084
	χ^2	0.040	0.028	0.028	0.030	0.047	0.062
	SAE	0.024	0.198	0.285	0.485	0.542	0.603
	ARE	0.025	0.258	0.365	0.610	0.615	0.782
	HYBRID	1.114	0.457	0.068	0.736	1.134	1.501
Dubinin–Radushkevich	k_{DR} (mol^2/J^2)	1.2E – 8	1.7E – 8	2.6E – 8	1.13 E – 8	1.11E – 8	1.07E – 8
	X_m (mg/g)	5.450	5.388	5.270	5.876	5.991	6.020
	E (kJ/mol)	6.190	6.042	4.404	9.368	9.425	9.836
	r^2	0.930	0.928	0.927	0.997	0.982	0.971
	sd	0.078	0.079	0.075	0.016	0.019	0.023
	χ^2	0.019	0.019	0.018	0.012	0.018	0.023
	SAE	0.026	0.078	0.215	0.014	0.075	0.135
	ARE	0.035	0.097	0.283	0.018	0.096	0.175
	HYBRID	0.445	0.452	0.442	0.210	0.452	0.790

Table 2
Thermodynamic parameters of Zr–Ox and Alg–Ox–Zr complex.

Thermodynamic parameters		Zr-Ox	Alg-Ox-Zr
ΔG^o (kJ mol^{-1})	303 K	−0.186	−1.265
	313 K	−0.527	−1.337
	323 K	−1.076	−1.492
ΔH^o (kJ mol^{-1})		13.060	2.159
ΔS^o (kJ mol^{-1}K^{-1})		0.044	0.011

3.7.1. Reaction-based models

The slope of the plot $\log(q_e - q_t)$ vs. t of pseudo-first-order equation (Lagergren, 1898) at different experimental conditions would give the values of the rate constant and were given in Table S2 and Table S3. Linear plots of $\log(q_e - q_t)$ vs. t indicated the applicability of Lagergren equation. The pseudo-second-order plot of t/q_t vs. t (Ho, 2006) resulted in a straight line with higher r values than the pseudo-first-order, which indicated the better applicability of pseudo-second-order model for both Alg–Ox–Zr and Zr–Ox complexes and the values were summarized in Table S2 and Table S3 respectively. The values of q_e increased with increase in initial fluoride concentration and also with increase in temperature which indicated the influence of chemisorption (Ganesan, Lakshmi, Sozhan, & Vasudevan, 2013; Vasudevan, Lakshmi, & Sozhan, 2013).

3.7.2. Diffusion-based models

In a solid–liquid sorption process, the transfer of solute was characterized by intra-particle diffusion (Weber & Morris, 1964) or particle diffusion (Wankasi, Horsfall, & Spiff, 2005) model. Both intra particle and particle diffusion models were applied for Alg–Ox–Zr as well as Zr–Ox complex and the values of rate constants k_i and k_p are presented in Table S2 and Table S3 respectively. Higher r values in both the cases indicated the possibility of sorption process being controlled by intra particle diffusion model for both the sorbents.

3.7.3. Fitness of sorption kinetic models

The kinetic models were evaluated for fitness of the sorption data by calculating the standard deviations (sd). Lower values of sd shows a better fitness of the sorption data (Ho et al., 2000). The sd values of reaction-based and diffusion-based models of both Alg–Ox–Zr and Zr–Ox complexes were computed and summarized in Table S2 and Table S3 respectively. Pseudo-second-order and intra-particle diffusion models possessed lower sd values than the pseudo-first-order and particle diffusion model. Hence, the pseudo-second-order and intra particle diffusion models were identified as the best fit for the sorption of fluoride onto the complexes.

3.8. Mechanism of fluoride removal

Fig. 6 depicts the fluoride removal mechanism using Alg–Ox–Zr complex. In the first step, hydrolysis of zirconium oxychloride leads to a tetramer complex formation which is surrounded by —OH groups and water molecules. Then, the zirconium complex gets coordinated to COO^- and OH^- group of alginate polymer during the addition of alginate and form an intermediate complex. In the next step, oxalic acid is added to the intermediate complex at 80 °C for 2 h; as a result, there is a formation of a six coordinate structure of zirconyl oxalate complex with the backbone of alginate (Jimenez et al., 2014; Muthu Prabhu & Meenakshi, 2015). The —COO^- and —OH groups in the alginate facilitate the formation of complexes with zirconium with oxalic acid. In the final step of the reaction, the fluoride ion tends to attack the —OH group, resulting in the formation of Zr–F by ligand-exchange mechanism. The formation of the fluoride coordinated complex is further supported by FTIR spectroscopy. The Zr–OH band at 1353 cm^{-1} has been shifted to 1315 cm^{-1} which is due to the formation of Zr–F complex and the band is very sharp. The EDAX spectra depict the percentage of oxygen content in the fluoride adsorbed complex, which has been decreased and thus indicates the presence of fluoride removal.

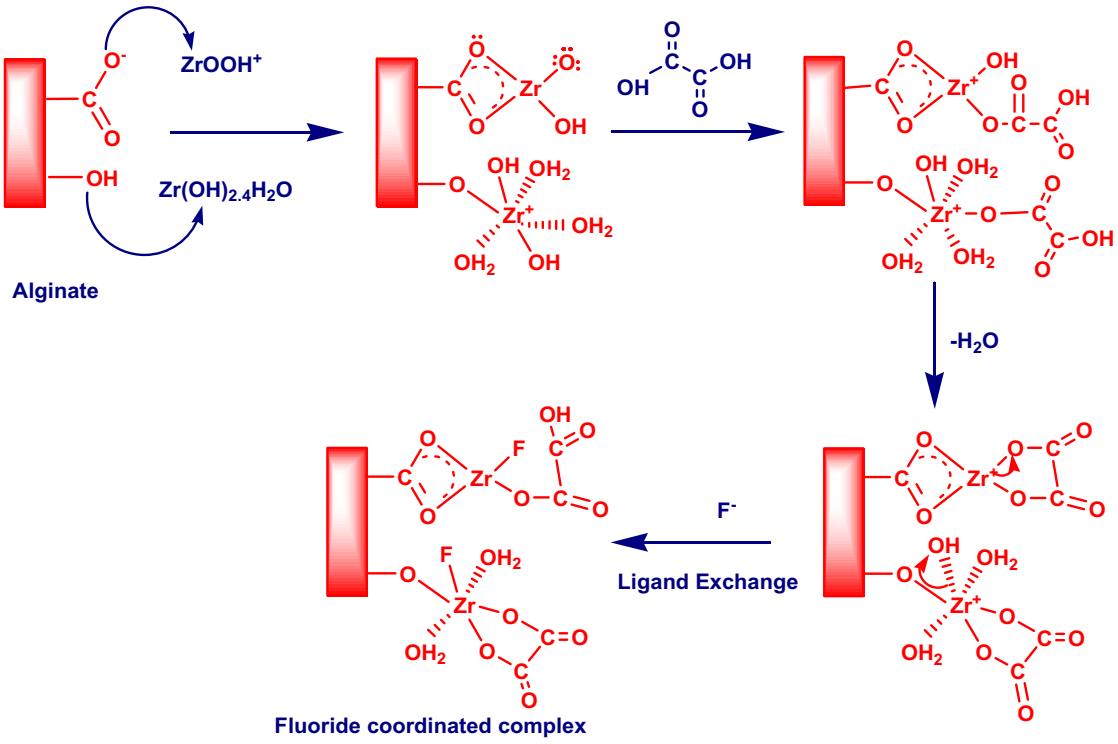

Fig. 6. Mechanism of fluoride removal.

A comparison has been made between Alg–Ox–Zr complex and previously reported adsorbents for fluoride removal and are presented in Table S4.

3.9. Testing with real water samples

The Alg–Ox–Zr complex possessed higher DC is also tested with field sample taken from a nearby fluoride-endemic village, namely Thomaiyarpuram, Dindigul District, Tamil Nadu, India. A minimum amount of sorbent was added to a 50 mL of water sample and the contents were shaken for a constant time at room temperature. These results are presented in Table S5. There is a significant reduction in the levels of other water quality parameters also in addition to fluoride. It is evident from the result that the sorbent, Alg–Ox–Zr complex can be effectively employed for removing the fluoride from water.

4. Conclusion

This research report demonstrates the removal of fluoride using Alg–Ox–Zr complex, which showed higher DC than the other dicarboxylic acids mediated zirconium encapsulated alginate complex from aqueous solution. When this complex was used to remove fluoride, the maximum DC obtained was 9653 mgF^-/kg and the adsorption of fluoride onto Alg–Ox–Zr complex was spontaneous and thermodynamically favorable. The studies on pH dependence, adsorption isotherms and co-existing anions have been conducted for optimization of fluoride removal from aqueous solution by both the complexes. Based on r^2, sd and error analysis values, the Freundlich isotherm model have been identified as the best fit for the fluoride adsorption onto Alg–Ox–Zr complex. The mechanism of fluoride removal using Alg–Ox–Zr complex was ligand-exchange which was supported by the various spectral methods like FTIR, XRD, SEM with EDAX and mapping study. The results of the present study with Alg–Ox–Zr complex indicate that this adsorbent has promising potential for fluoride remediation.

Acknowledgment

The first author, S. Muthu Prabhu likes to thank University Grants Commission-Research Fellowship in Sciences for Meritorious Students, New Delhi, India for providing of financial support to carry out this research work.

Appendix A. Supplementary data

Supplementary data associated with this article can be found, in the online version, at http://dx.doi.org/10.1016/j.carbpol.2014.11.058.

References

APHA. (2005). *Standard methods for the examination of water and waste water*. Washington, DC: American Public Health Association.
Barbier, O., Arreola-Mendoza, L., & Razo, L. M. D. (2010). Molecular mechanisms of fluoride toxicity. *Chemico-Biological Interactions*, *188*, 319–333.
Basu, H., Singhal, R. K., Pimple, M. V., & Reddy, A. V. R. (2013). Synthesis and characterization of alumina impregnated alginate beads for fluoride removal from potable water. *Water Air & Soil Pollution*, *224*, 1572–1584.
Cao, J. L., Chen, J. J., Wang, J. D., Jia, R. H., Xue, W. J., Luo, Y. J., et al. (2013). Effects of fluoride on liver apoptosis and Bcl-2, Bax protein expression in freshwater teleost cyprinus carpio. *Chemosphere*, *91*, 1203–1212.
Cheng, Z. H., Yasukawa, A., Kandori, K., & Ishikawa, T. (1998). FTIR Study on incorporation of CO_2 into calcium hydroxyapatite. *Journal of the Chemical Society Faraday Transactions*, *94*, 1501–1505.
Fluoride. (2005). *Electrode Instruction Manual*. USA: Orion Research.
Freundlich, H. M. F. (1906). Uber die adsorption in lösungen. *International Journal of Research in Physical Chemistry and Chemical Physics*, *57A*, 385–470.
Ganesan, P., Lakshmi, J., Sozhan, G., & Vasudevan, S. (2013). Removal of manganese from water by electrocoagulation: Adsorption, kinetics and thermodynamic studies. *Canadian Journal of Chemical Engineering*, *91*, 448–458.
Guo, G. Y., & Chen, Y. L. (2004). New zirconium hydroxide. *Journal of Materials Science*, *39*, 4039–4043.
Ho, Y. S., Ng, J. C. Y., & McKay, G. (2000). Kinetics of pollutant sorption by biosorbents: Review. *Separation and Purification Methods*, *29*, 189–232.
Ho, Y. S., Chiu, W. T., & Wang, C. C. (2005). Regression analysis for the sorption isotherms of basic dyes on sugarcane dust. *Bioresource Technology*, *96*, 1285–1291.

Ho, Y. S. (2006). Second order kinetic model for the sorption of cadmium onto tree fern: A comparison of linear and non linear methods. *Water Research*, *40*, 119–125.

Horsfall, M., & Spiff, A. I. (2005). Effects of temperature on the sorption of Pb^{2+} and Cd^{2+} from aqueous solution by caladium bicolor (Wild Cocoyam) biomass. *Journal of Biotechnology*, *8*, 162–169.

Jimenez, L. H. V., Hurt, R. H., Matos, J., & Mendez, J. R. R. (2014). Zirconium-carbon hybrid sorbent for removal of fluoride from water: Oxalic acid mediated zr(IV) assembly and adsorption mechanism. *Environmental Science & Technology*, *48*, 1166–1174.

Ketabi, S. A., Kazemi, A. S., & Mohagheghi, M. M. B. (2011). The effect of complexing agent on the crystallization of ZnO nanoparticles. *Journal of Physics (Paris)*, *77*, 679–688.

Khan, A. A., & Singh, R. P. (1987). Adsorption thermodynamics of carbofuran on Sn(IV) arsenosilicate in H^+, Na^+ and Ca^{2+} forms. *Colloids and Surfaces*, *24*, 33–42.

Koji, M., & Ohgai, M. (2001). Formation mechanism of hydrous zirconia particles produced by the hydrolysis of $ZrOCl_2$ solutions: III, kinetics study for the nucleation and crystal-growth processes of primary particles. *Journal of the American Ceramic Society*, *84*, 2303–2312.

Kundu, S., & Gupta, A. K. (2006). Arsenic adsorption onto iron oxide-coated cement (IOCC): Regression analysis of equilibrium data with several isotherm models and their optimization. *Chemical Engineering Journal*, *122*, 93–106.

Kurkuri, M. D., Kumbar, S. G., & Aminabhavi, T. M. (2002). Synthesis and characterization of polyacrylamide-grafted sodium alginate copolymeric membranes and their use in pervaporation separation of water and tetrahydrofuran mixtures. *Journal of Applied Polymer Science*, *86*, 272–281.

Lagergren, S. (1898). Zur theorie der sogenannten adsorption gelöster stoffe. *Kungliga Svenska Vetenskapsakademiens*, *24*, 1–39.

Langmuir, I. (1916). The constitution and fundamental properties of solids and liquids. *Journal of American Chemical Society*, *38*, 2221–2295.

Lee, K. Y., & Mooney, D. J. (2012). Alginate: Properties and biomedical applications. *Progress in Polymer Science*, *37*, 106–126.

Meenakshi, S., & Viswanathan, N. (2007). Identification of selective ion-exchange resin for fluoride sorption. *Journal of Colloid Interface Science*, *308*, 438–450.

Milmile, S. N., Pande, J. V., Karmakar, S., Bansiwal, A., Chakrabarti, T., & Biniwale, R. B. (2011). Equilibrium isotherm and kinetic modeling of the adsorption of nitrates by anion exchange indion NSSR resin. *Desalination*, *276*, 38–44.

Mohapatra, M., Anand, S., Mishra, B. K., Giles, D. E., & Singh, P. (2009). Review of fluoride removal from drinking water. *Journal of Environmental Management*, *91*, 67–77.

Muthu Prabhu, S., & Meenakshi, S. (2015). Chemistry of defluoridation by one-pot synthesized dicarboxylic acids mediated polyacrylamide-zirconium complex. *Chemical Engineering Journal*, *262*, 224–234.

Pandi, K., & Viswanathan, N. (2014). Synthesis of alginate bioencapsulated nano-hydroxyapatite composite for selective fluoride sorption. *Carbohydrate Polymers*, *112*, 662–667.

Park, H. G., & Chae, M. Y. (2004). Novel type of alginate gel-based adsorbents for heavy metal removal. *Journal of Chemical Technology and Biotechnology*, *79*, 1080–1083.

Paudyal, H., Pangeni, B., Inoue, K., Kawakita, H., Ohto, K., Ghimire, K. N., et al. (2013). Preparation of novel alginate based anion exchanger from Ulva japonica and its application for the removal of trace concentrations of fluoride from water. *Bioresource Technology*, *148*, 221–227.

Pettibone, J. M., Cwiertny, D. M., Sherer, M., & Grassian, V. H. (2008). Adsorption of organic acids on TiO2 nanoparticles: effects of pH, nanoparticle size and particle aggregation. *Langmuir*, *24*, 6659–6667.

Polyak, B., Geresh, S., & Marks, R. S. (2004). Synthesis and characterization of a biotin-alginate conjugate and its application in a biosensor construction. *Biomacromolecules*, *5*, 389–396.

Ramosa, R. L., Utrilla, J. R., Castilloa, N. A. M., & Polo, M. S. (2010). Kinetic modeling of fluoride adsorption from aqueous solution onto bone char. *Chemical Engineering Journal*, *158*, 458–467.

Socrates, G. (2001). *Infrared and Raman characteristic group frequencies. Tables and Charts* (3rd ed.). USA: Wiley.

Sundaram, C. S., & Meenakshi, S. (2009). Fluoride sorption using organic–inorganic hybrid type ion exchangers. *Journal of Colloid Interface Science*, *333*, 58–62.

Swaina, S. K., Patnaik, T., Patnaik, P. C., Jha, U., & Dey, R. K. (2013). Development of new alginate entrapped Fe(III)–Zr(IV) binary mixed oxide for removal of fluoride from water bodies. *Chemical Engineering Journal*, *215-216*, 763–771.

Trandafilović, L. V., Whiffen, R. K., Branković, S. D., Stoiljković, M., Luyt, A. S., & Djoković, V. (2014). ZnO/Ag hybrid nanocubes in alginate biopolymer: Synthesis and properties. *Chemical Engineering Journal*, *253*, 341–349.

Vani, M. L., & Reddy, K. P. (2000). Effects of fluoride accumulation on some enzymes of brain and gastrocnemius muscle of mice. *Fluoride*, *33*, 17–26.

Vasudevan, S., Lakshmi, J., & Sozhan, G. (2013). Electrochemically assisted coagulation for the removal of boron from water using zinc anode. *Desalination*, *310*, 122–129.

Vijaya, Y., Popuri, S. R., Reddy, A. S., & Krishnaiah, A. (2011). Synthesis and characterization of glutaraldehyde-crosslinked calcium alginate for fluoride removal from aqueous solutions. *Journal of Applied Polymer Science*, *120*, 3443–3452.

Viswanathan, N., & Meenakshi, S. (2008). Selective sorption of fluoride using Fe(III) loaded carboxylated chitosan beads. *Journal of Fluorine Chemistry*, *129*, 503–509.

Wankasi, D., Horsfall, M., & Spiff, A. I. (2005). Retention of Pb(II) ion from aqueous solution by nipah palm (nypa fruticans wurmb) petiole biomass. *Journal of the Chilean Chemical Society*, *50*, 691–696.

Weber, T. W., & Chakravorti, R. K. (1974). Pore and solid diffusion models for fixed bed adsorbers. *Journal of American Institute of Chemical Engineers*, *20*, 228–234.

Weber, W. J., & Morris, J. C. (1964). Equilibria and capacities for adsorption on carbon. *Journal of the Sanitary Engineering Division*, *90*, 79–91.

WHO. (2006). *Chemical fact sheets: Fluoride. Guidelines for drinking water quality: Incorporation first addendum*. Geneva: Recommendations.

Yakun, H., Wenming, D., Xia, H., Jingnian, X., & Menghua, Z. (2011). Fluoride removal by lanthanum alginate bead: adsorbent characterization and adsorption mechanism. *Chinese Journal of Chemical Engineering*, *19*, 365–370.